A Thermal System Model for a Radiant-Tube Continuous Reheating Furnace

H. Ramamurthy, S. Ramadhyani, and R. Viskanta

A thermal system mathematical model developed for a gas-fired radiant-tube continuous reheating furnace is discussed. The mathematical model of the furnace integrates submodels for combustion and heat transfer within the radiant tube with models for the furnace enclosure. The transport processes occurring in the radiant tube are treated using a one-dimensional scheme, and the radiation exchange between the load, the radiant-tube surfaces, and the furnace refractories are analyzed using the radiosity method. The continuous furnace operation is simulated under steady-state conditions. Model simulations of load surface temperature variation compare well with measurements in an industrial galvannealing furnace. The scope and flexibility of the model are assessed by performing extensive parametric studies using furnace geometry, material properties, and operating conditions as input parameters in the model and predicting the thermal performance of the furnace. The various parameters studied include the effects of load and refractory emissivities, load velocities, properties of the stock material, and variations in the radiant-tube designs.

Keywords
heat transfer, heating furnaces, process modeling, thermal modeling

1. Introduction

INDIRECTLY fired radiant-tube furnaces are widely used in metal heat-treating applications where the quality of the final heated product is a major concern (Ref 1). A typical radiant-tube continuous furnace employed for such applications is shown schematically in Fig. 1. In this type of furnace, the combustion of fuel and air takes place within the radiant tubes, and the high-temperature products of combustion are kept isolated from the stock material being heated (the load in Fig. 1). The energy released due to combustion is transferred to the radiant-tube wall, and the heating of the stock material is accomplished via radiative heat transfer from the heated walls of the radiant tubes and from other surfaces of the furnace enclosure. Furthermore, the furnace enclosure may be filled with an inert radiatively nonparticipating atmosphere, such as nitrogen or argon, to prevent scaling or decarburization of the load during the heating process (Ref 1).

A continuous furnace is typically equipped with several radiant tubes, and the stock material is transported through the furnace on conveyor belts or rollers (Fig. 1). The load in the furnace may be heated symmetrically from above and below by an identical set of radiant tubes, although Fig. 1 shows only the up-

H. Ramamurthy (presently at College of Engineering, University of California, Riverside, CA, USA), **S. Ramadhyani,** and **R. Viskanta,** Heat Transfer Laboratory, School of Mechanical Engineering, Purdue University, West Lafayette, IN 47907, USA

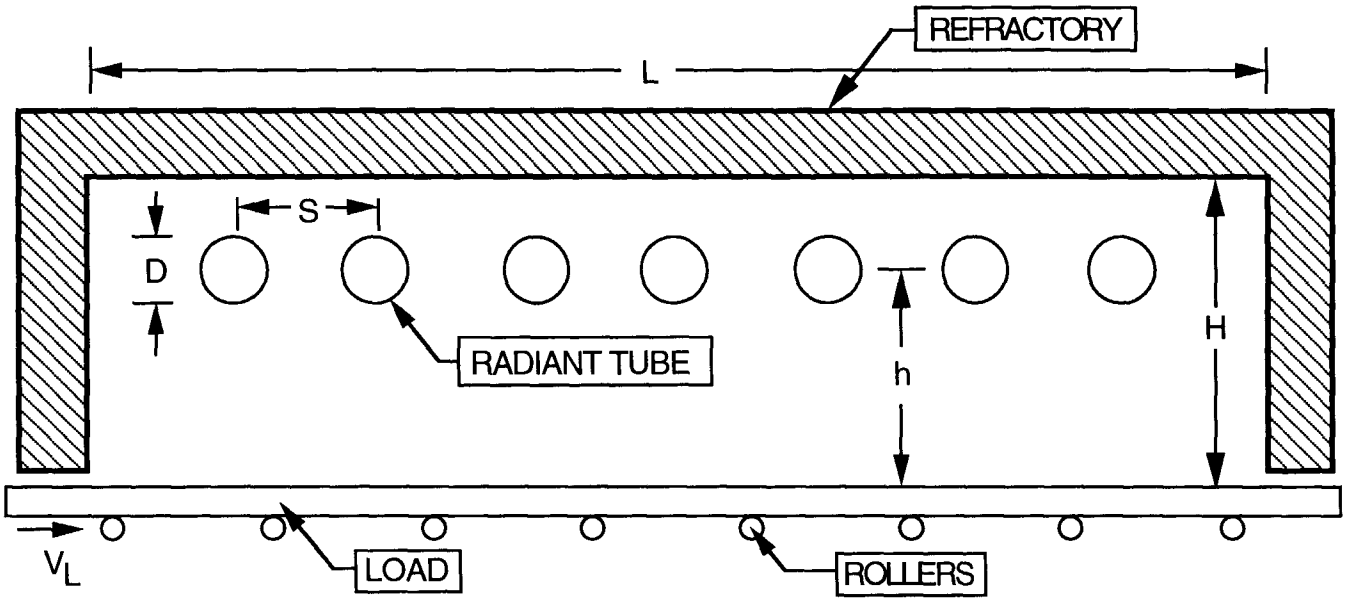

Fig. 1 Physical model of a radiant-tube continuous furnace

per half of the furnace. The primary objectives in the operation of a continuous furnace are to maximize the mass throughput of stock material and to maximize the heat transfer to the load due to the combustion of fuel in the radiant tubes. However, attempts to maximize the throughput may adversely affect the maximum heat transfer to the load, and vice versa. Therefore, it becomes necessary to optimize the furnace operation for the most efficient heat transfer and greatest throughput. This can be accomplished by conducting numerical experiments using a thermal system mathematical model of the furnace. The mathematical model developed in this study provides for detailed simulations of the heat-transfer processes occurring in the furnace and uses design, operating conditions, and material properties of the furnace as inputs to examine their effects on furnace operation. A detailed parametric analysis of the furnace is then performed to reveal important trends and design conditions for the furnace and to identify means of optimizing furnace performance.

Before discussing the mathematical model of the furnace, we will outline the details of the heat-transfer processes occurring within the furnace. The various modes of heat transfer in a radiant-tube continuous furnace are depicted schematically in Fig. 2. Fuel (natural gas) and air enter the radiant tube through a coaxial-diffusion flame burner installed at one end of the tube. The two streams mix with each other by turbulent diffusion; combustion occurs in the mixing zone, leading to the formation of a flame. The high-temperature products of combustion transfer a portion of their energy to the radiant-tube wall by convection and radiation, and a portion of the energy leaving the radiant-tube exhaust is recovered in a recuperator. Radiation is the primary mode of heat transfer from the combustion products to the tube wall (Ref 2, 3). The products of combustion of natural gas include strongly radiating species, such as CO_2 and H_2O, that are spectrally selective absorbers and emitters of thermal radiation (Ref 4, 5). The high-temperature radiant-tube wall then transfers heat to the load, the refractory walls, and the adjacent radiant tubes in the furnace. A portion of the energy incident on these surfaces is absorbed, and the remainder is reflected back into the furnace enclosure. The absorbed energy raises the temperature of the surface, which then reradiates to the other surfaces of the enclosure. Additionally, the motion of the load through the furnace induces circulation of the furnace gases; this helps to transfer heat by convection to the various surfaces of the enclosure. The heat transferred to the refractory walls is then conducted through the wall material and lost to the ambient atmosphere by convection and radiation. The heat incident on the load is redistributed within the load by conduction as well as advection caused by the movement of the load within the furnace.

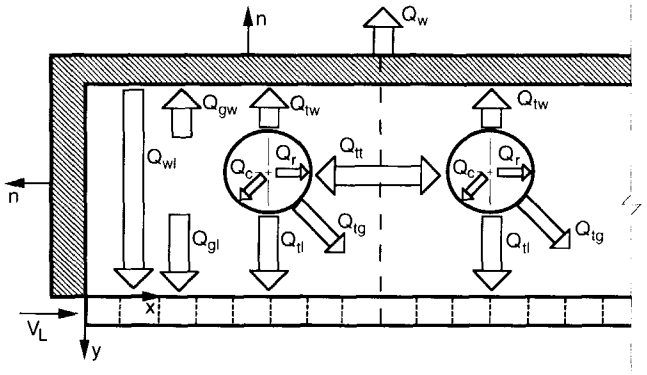

Fig. 2 Modes of heat transfer in a radiant-tube continuous furnace

2. Mathematical Model

The thermal system model for the radiant-tube continuous furnace involves integration of the mathematical models of the furnace enclosure and of the radiant tube (Ref 6). The furnace-enclosure model calculates the heat transfer and the temperature distribution in the load, the refractory walls, and the furnace gas. The radiant-tube model simulates the turbulent transport processes, the combustion of fuel and air, and the convective and radiative heat transfer from the combustion products to the tube wall in order to calculate the local radiant-tube wall and gas temperatures. Integration of the furnace-enclosure model and the radiant-tube model is achieved using the radiosity method (Ref 5). Brief discussions of the individual submodels that constitute the furnace-enclosure and the radiant-tube models and their integration into a thermal system mathematical model are presented in the following sections.

2.1 *Furnace Zoning*

In order to simplify the complex heat-transfer processes occurring within the furnace, the surface areas of the furnace enclosure are subdivided into smaller zones that are assumed to be isothermal (Ref 4). Energy balances are then applied to each zone, resulting in a set of simultaneous equations that are solved to determine the temperature and heat fluxes in each zone.

For the zonal analysis of the furnace, the enclosure is divided into N major zones, where N represents the number of radiant tubes in the furnace. The furnace gas within the enclosure is thus subdivided into N gas volume zones. The furnace roof (or crown), the front wall, and the back wall are each subdivided into N isothermal surface zones, and each end wall of the furnace is modeled as a single isothermal surface zone. Although the radiant-tube wall temperature varies axially along the length of the tube, the exterior surface of each radiant tube is treated as an isothermal surface zone at an average tube wall temperature. The zonal analysis thus results in $5 \times N + 2$ major surface zones and N gas volume zones. The load zones are further subdivided into smaller control volumes (Fig. 2) to resolve more accurately the temperature variations in the load.

2.2 *Radiosity Method*

All surfaces of the furnace enclosure are assumed to be diffuse and gray emitters and reflectors of radiation. For an enclosure consisting of M surface zones with known surface temperatures, the radiosity equation for each surface zone k is written as (Ref 5):

$$\sum_{j=1}^{M} [\delta_{kj} - (1 - \varepsilon_k) F_{k-j}] J_j = \varepsilon_k \sigma \bar{T}_k^4 \qquad 1 \le k \le M \quad \text{(Eq 1)}$$

where J_j represents the radiosity at surface j, $\bar{T}_k$ represents the average surface temperature of zone k, and F_{k-j} represents the view factor between surfaces k and j.

The foregoing set of radiosity equations can be readily solved for the unknown radiosities using a matrix inversion procedure (Ref 5). The net average heat flux leaving each surface zone is then obtained from the radiosities as:

$$\bar{q}_{\text{tot},k} = \frac{\varepsilon_k}{(1-\varepsilon_k)} [\sigma \bar{T}_k^4 - J_k] + \bar{h}_k (\bar{T}_k - \bar{T}_{g,k})$$

$$1 \le k \le M \qquad \text{(Eq 2)}$$

where $\bar{h}_k$ is the average convective heat-transfer coefficient at surface k, and $\bar{T}_{g,k}$ is the average gas temperature in the furnace gas zone with which the kth surface zone is in contact. This temperature is obtained from the furnace gas model. As noted earlier, the radiant-tube wall temperature varies axially along the length of the tube, but an average tube wall temperature is used for the solution of the radiosity equations. The computation of the average tube wall temperature is discussed in section 2.5.

2.3 *Furnace-Enclosure Model*

The furnace-enclosure model mathematically models the heat transfer in the load, the refractory walls, and the furnace gas.

2.3.1 Load Model

The two-dimensional steady-state energy equation of the load is written as (Ref 7, 8):

$$\frac{\partial}{\partial_x}(\rho_L C_L V_L T_L) = \frac{\partial}{\partial_y}\left(k_L \frac{\partial T_L}{\partial y}\right) \qquad \text{(Eq 3)}$$

where V_L is the velocity of the load (Fig. 2). In deriving Eq 3, conduction along the x-direction is neglected in comparison to that along the y-direction due to the large length-to-thickness ratio of the load ($L_L/t_L \approx 500$).

The boundary condition at the inner (top) surface of the load zones exposed to the heat flux from the radiant tubes and the furnace walls is

$$-k_L \frac{\partial T_L}{\partial y}\bigg|_{\text{inner } (y=0)} = -\bar{q}_{\text{tot}} \qquad \text{(Eq 4)}$$

where $\bar{q}_{\text{tot}}$ is the average heat flux in each load zone obtained from Eq 2. Due to symmetric heating of the load from above and below, the midplane of the load is considered a plane of symmetry, and the boundary condition is expressed as:

$$\frac{\partial T_L}{\partial y}\bigg|_{\text{midplane}} = 0 \qquad \text{(Eq 5)}$$

The temperature of the load entering the furnace is known and is used as an initial condition for the x-direction:

$$T_L\big|_{(x=0)} = T_{\text{known}} \qquad \text{(Eq 6)}$$

2.3.2 Refractory Wall Model

The energy equation for the furnace refractory wall zones is similar to that for the load zones, except for the advection term. The one-dimensional steady-state heat conduction equation for the furnace walls is written as (Ref 7, 8):

$$\frac{\partial}{\partial n}\left(k_w \frac{\partial T_w}{\partial n}\right) = 0 \qquad \text{(Eq 7)}$$

where n represents the direction of the exterior normal to the walls (Fig. 2). The boundary condition on the inner surface of the refractory wall zones is the imposed heat flux condition, expressed as:

$$-k_w \frac{\partial T_w}{\partial n}\bigg|_{\text{inner}} = -\bar{q}_{\text{tot}} \qquad \text{(Eq 8)}$$

and the boundary condition on the outer surface of the furnace walls exposed to the ambient surroundings is given by:

$$-k_w \frac{\partial T_w}{\partial n}\bigg|_{\text{outer}} = \bar{h}(T_{w,\text{outer}} - T_{\text{amb}}) \qquad \text{(Eq 9)}$$

where $\bar{h}$ is an effective (convective plus radiative) heat-transfer coefficient, and T_{amb} is the ambient temperature.

2.3.3 Furnace Gas Model

The furnace gas in each gas zone is assumed to be radiatively nonparticipating and to be "well stirred"øthat is, to have a uniform gas composition and temperature. The energy equation for the furnace gas in the kth gas zone is written as:

$$\sum_{l=1}^{s} \bar{h}_l A_l [\bar{T}_{g,k} - \bar{T}_l] = 0 \qquad \text{(Eq 10)}$$

where s is the total number of surface zones with which the kth gas zone is in contact, and $\bar{h}_l$ represents the corresponding average convective heat-transfer coefficient specified along the inner surfaces of the furnace enclosure.

2.4 *Radiant-Tube Model*

The mathematical model of a radiant tube entails detailed numerical modeling of combustion, radiation, and the turbulent transport of mass, momentum, chemical species, and energy within the tube. Such a task, using a two-dimensional, axisymmetric model for the radiant tube is computationally intensive, requiring the simultaneous solution of several coupled nonlinear partial differential equations (Ref 8, 9). Conse-

quently, for the purposes of the thermal system model of the furnace, the basic transport processes within the radiant tube are treated in a plug-flow fashion using a one-dimensional scheme. A one-dimensional radiant-tube model, similar to those employed by Lisienko et al. (Ref 10) and Harder et al. (Ref 3), which takes into account turbulence, flow relaminarization, combustion, and radiation occurring within the radiant tube, is used in the present study for the furnace thermal system model.

The one-dimensional model allows for the calculation of the convective and radiative heat flux from the radiant tube as well as the local variations in the tube wall and the combustion gas temperatures in the tube. For steady plug-flow through the radiant tube, the basic conservation equations representing the transport of mass, momentum, and energy of the radiant tube gases are, respectively (Ref 3):

$$\frac{d(\rho V)}{dz} = 0 \qquad \text{(Eq 11)}$$

$$\rho V \frac{dV}{dz} + \frac{dp}{dz} + \frac{2}{R_i}\tau = 0 \qquad \text{(Eq 12)}$$

$$\frac{d}{dz}(\dot{m}h^{a}) = h_i P_i (T_{tw} - T_{cg}) - \Delta H_{fu}\frac{d\dot{m}_{fu}}{dz} - P_i q_{rad,i} \qquad \text{(Eq 13)}$$

where h^a is the sensible enthalpy of the mixture, ΔH_{fu} is the heat of reaction between fuel and oxidant, and τ is the shear stress expressed in terms of the Darcy friction factor, f_D, as:

$$\tau = \left(\frac{\rho V^2}{8}\right) f_D \qquad \text{(Eq 14)}$$

The radiant-tube gases at any axial location z are assumed to consist of a combination of three species: fuel, air, and combustion products. The proportions of each of these species can be determined from a fuel burnup coefficient, which represents the fraction of the initial fuel consumed during the combustion process (Ref 10). The mass flow rates of the three species—fuel, air, and combustion products—at any axial location z can then be obtained from:

$$\dot{m}_{fu}(z) = \dot{m}_{fu}(0)[1 - \kappa(z)] \qquad \text{(Eq 15)}$$

$$\dot{m}_{a}(z) = \dot{m}_{a}(0)[1 - \Phi\kappa(z)] \qquad \text{(Eq 16)}$$

$$\dot{m}_{pr}(z) = \dot{m}_{a}(0) + \dot{m}_{fu}(0) - \dot{m}_{fu}(z) - \dot{m}_{a}(z) \qquad \text{(Eq 17)}$$

The sensible enthalpy of the mixture, which is a function of the local gas temperature, is determined from:

$$\dot{m}h^{a} = \dot{m}_{fu}\int_{T_{ref}}^{T_{cg}} C_{p,fu}(T)dT + \dot{m}_{a}\int_{T_{ref}}^{T_{cg}} C_{p,a}(T)dT + \dot{m}_{pr}\int_{T_{ref}}^{T_{cg}} C_{p,pr}(T)dT \qquad \text{(Eq 18)}$$

where temperature-dependent specific heat values are used for fuel, air, and combustion products (Ref 1).

A correlation for the fuel burnup coefficient, κ, was developed by Lisienko et al. (Ref 10) based on the results of a two-dimensional flow and combustion analysis in a straight-through type of radiant tube. The fuel burnup coefficient was obtained as a function of axial position, tube diameter, and the Reynolds number of flow and is given by:

$$\kappa(z) = \left[1 - \exp\left(-4\frac{z}{D}\mathrm{Re}_D^{-0.3}\right)\right] \qquad \text{(Eq 19)}$$

This correlation, however, did not take into account the effect of operating conditions—such as burner geometry, air-fuel ratio, and combustion air preheat temperature—on fuel burnup. Ramamurthy (Ref 8) recently developed correlations for fuel burnup and wall heat transfer based on the two-dimensional analysis of long diffusion flames in radiant tubes for varying tube operating conditions. The fuel burnup coefficient (Ref 8) was expressed as:

$$\kappa(z) = 1 - \exp\left[-8.24 \times 10^{-4}\frac{\mathrm{AR}^{0.54}}{\Phi^{1.53}}P_r^{0.41}\left(\frac{z}{D}\right)^{1.6}\mathrm{Re}_{FT}^{-0.08}\right] \qquad \text{(Eq 20)}$$

where Re_{FT} represents the Reynolds number of flow evaluated at the stoichiometric adiabatic flame temperature of the fuel, and P_r represents the momentum ratio between the air and fuel streams at the burner inlet. A comparison of the two fuel burnup correlations revealed that despite the simplicity of the Lisienko et al. (Ref 10) correlation, it modeled short flames generated by high-intensity diffusion flame burners in straight-through radiant tubes fairly well (Ref 8). Therefore, for consistency in the comparison of flames generated by different radiant-tube burners, the Lisienko et al. (Ref 10) fuel burnup correlation is adopted in the present modeling study.

For predicting convective heat transfer from the combusting, reacting, and developing flow in the radiant tube, a modified form of the convective correlation proposed by Gnielinski (Ref 11) is used. The convective heat-transfer coefficient, written in terms of Nusselt number, is expressed as:

$$h_i D_i / k_{cg} = \mathrm{Nu}_{D_i} = \frac{C_c(f_D/8)(\mathrm{Re}_D - 1000)\,\mathrm{Pr}}{1 + 12.7(f_D/8)^{1/2}\left(\mathrm{Pr}^{2/3} - 1\right)} \qquad \text{(Eq 21)}$$

where

$$f_D = (0.79 \ln \mathrm{Re}_D - 1.64)^{-2} \qquad \text{(Eq 22)}$$

and C_c represents a suitable multiplication factor that modifies the Gnielinski correlation to account for effects of flow development and combustion (for details, see Ref 8).

For predicting radiative heat transfer, the combustion gases are treated as an absorbing-emitting and nonscattering medium, and gas emittance and absorptance are taken to be dependent on both temperature and the pressure-path length product as discussed by Hottel (Ref 12). The radiant heat flux from the combustion products to the inner tube wall was obtained by modifying Hottel's correlation and is given by:

$$q_{\text{rad,i}} = \frac{C_r \varepsilon_{\text{tw,i}} \sigma (\varepsilon_{\text{cg}} T_{\text{cg}}^4 - \alpha_{\text{cg}} T_{\text{tw}}^4)}{1 - (1 - \varepsilon_{\text{tw,i}})(1 - \alpha_{\text{cg}})} \quad \text{(Eq 23)}$$

where T_{cg} represents the local mean combustion gas temperature, T_{tw} is the local tube wall temperature, and C_r is a suitable multiplication factor to account for the nonuniformity of the combustion gas temperature (Ref 8).

Heat transfer to the tube wall is assumed to occur only in the radial direction, as expressed by Eq 13. Because the radiant tube wall is relatively thin compared to the tube length ($t_t/L_t < 0.02$), axial heat conduction along the tube wall is neglected. Thus, for each control volume, an energy balance on the tube wall yields:

$$h_i(T_{\text{cg}} - T_{\text{tw}}) + q_{\text{rad,i}} = \frac{R_o}{R_i}\left[h_o (T_{\text{tw}} - \bar{T}_{\text{g,k}}) + q_{\text{rad,o}}\right] \quad \text{(Eq 24)}$$

where $\bar{T}_{\text{g,k}}$ is the gas temperature in the furnace gas zone that is in contact with the radiant tube.

Assuming that the forced circulation of the furnace gases is relatively feeble, the flow around the radiant tube will be dominated by natural convection. The external convective heat-transfer coefficient, h_o, was obtained via an expression by Morgan (Ref 13) and is written as:

$$\frac{h_o D_o}{k_g} = \text{Nu}_{D_o} = C_n \text{Ra}_{D_o}^n \quad \text{(Eq 25)}$$

where k_g is the thermal conductivity of the furnace gas calculated at the mean film temperature, Ra_{D_o} is the Rayleigh number based on the tube outer diameter, and C_n and n are constants over a range of Rayleigh number values (Ref 14).

Radiant heat-transfer rate from the outer surface of the tube to the furnace enclosure is calculated by treating the tube as a small object in a large isothermal enclosure and for each control volume in the radiant tube is expressed as (Ref 4):

$$q_{\text{rad,o}} = \varepsilon_{\text{tw,o}} \sigma (T_{\text{tw}}^4 - \bar{T}_{\text{en}}^4) \quad \text{(Eq 26)}$$

where $\bar{T}_{\text{en}}$ is the mean enclosure temperature. Calculation of the mean enclosure temperature is discussed later in this paper.

2.5 *Method of Solution*

The first step in the solution procedure involves the zoning of the furnace into isothermal surface and volume zones. The next step involves the calculation of the configuration factors (F_{k-j}) between various isothermal surface zones of the furnace. These are evaluated using analytical expressions provided by Siegel and Howell (Ref 5) for generic surface configurations and employing integral expressions given by Sparrow and Cess (Ref 15) for more complicated geometries. The expressions for configuration factors are evaluated using numerical integration techniques.

The initial temperatures of all surface and gas volume zones of the furnace, including the outer surface of the radiant tubes, are specified. The convective heat-transfer coefficient on each surface of the enclosure is estimated using empirical expressions for flow over flat vertical and horizontal plates and for flow over a bundle of tubes (Ref 14). The furnace gas model (Eq 10) is first solved to obtain the average gas temperature, $\bar{T}_{\text{g,k}}$, in each gas volume zone. For specified radiative properties in each surface zone, the radiosity equation (Eq 1) is then solved using a matrix inversion routine, and the average radiative and convective heat fluxes leaving each surface zone are obtained from Eq 2. The net average heat flux, $\bar{q}_{\text{tot}}$, serves as the boundary condition in the solution of the respective energy equations for the load and the furnace refractory walls (Eq 3 and 7). The heat flux in Eq 2 is a nonlinear function of the surface temperature; therefore, in the solution of the energy equations, it is linearized using a first-order Taylor series expansion of the heat flux about the surface temperature. The energy equations are then solved for the temperature distribution in the load and refractory walls using the tridiagonal matrix algorithm (TDMA) with linearized source terms (Ref 16).

Equations 11 to 13 along with the ideal gas equation of state are solved using a predictor-corrector routine for radiant-tube gas temperature, velocity, pressure, and density. Employing an underrelaxed Newton-Raphson technique, Eq 24 can be solved for the local tube wall temperature during each predictor-corrector step, provided that the mean enclosure temperature, $\bar{T}_{\text{en}}$, and hence the radiative heat flux from the outer surface of the tube in Eq 26 are known.

Radiation is the dominant mode of heat transfer from the radiant tubes to the different surfaces of the furnace enclosure (Ref 3). Thus, from the specified average surface temperature of the tube and the average radiative heat flux from the tube, $\bar{q}_{\text{rad,t}}$, obtained from Eq 1, the enclosure temperature for each radiant tube is determined from:

$$\bar{q}_{\text{rad,t}} = \varepsilon_{\text{tw,o}} \sigma (\bar{T}_{\text{tw}}^4 - \bar{T}_{\text{en}}^4) \quad \text{(Eq 27)}$$

Using the enclosure temperatures, the solution of the radiant-tube model yields the local gas and tube wall temperatures and the net local heat flux at the radiant-tube surface. The heat flux obtained from the radiant-tube model has to be consistent with the heat flux determined from the radiosity method for the specified average tube wall temperature. Therefore, the sum of the local radiative heat fluxes from each control volume should

equate to the net radiative heat flux from the tube obtained from the radiosity method. Thus,

$$\sum_i q_{rad,o}\,\Delta z_i = \bar{q}_{rad,t} L_t \qquad \text{(Eq 28)}$$

where L_t is the axial length of the radiant tube and Δz_i is the axial step size. Upon substituting for $q_{rad,o}$ from Eq 26 and $\bar{q}_{rad,t}$ from Eq 27, the relationship between the average tube wall temperature and the local tube wall temperatures is

$$\bar{T}^4_{tw} = \frac{1}{L_t}\sum_i T^4_{tw,i}\,\Delta z_i \qquad \text{(Eq 29)}$$

The calculation of the average tube wall temperature using Eq 29 ensures consistency between the radiative heat fluxes from each radiant tube obtained from the radiant-tube model and from the radiosity method.

The temperature distributions in all the surface zones and gas volume zones are thus obtained. In the continuous furnace, each load zone is subdivided into smaller control volumes (Fig. 2); therefore, an average temperature for the load zone is obtained by averaging the surface temperatures of each control volume in a load zone. The new average values of furnace gas temperature, radiant-tube wall, furnace wall, and load surface temperatures are used in Eq 1 to recalculate the surface radiosities and hence the heat fluxes. This procedure is repeated until a converged steady-state solution for the continuous furnace is obtained. The thermophysical properties, such as thermal conductivity, volumetric heat capacity (ρC), and emissivity, for these materials are listed in Table 1. The model uses temperature-dependent thermal conductivity for all materials, but assumes volumetric heat capacity and emissivity of the surfaces to be constants and independent of temperature. Table 2 lists furnace operating conditions and dimensions.

3. Continuous Furnace Model Validation

The thermal system model developed for the radiant-tube continuous furnace was validated using experimental data obtained on an industrial galvannealing furnace at Inland Steel Corporation (East Chicago, Indiana) (Ref 17). A schematic of the furnace is shown in Fig. 3. A steel strip moving on top of rollers was initially heated to a high temperature in the direct-fired section of the furnace and then soaked in the indirect-fired section. The indirect-fired section was equipped with 64 U-type radiant tubes, with 32 radiant tubes above the load and 32 below it. The furnace was approximately 27 m long, 2.9 m wide, and 2.4 m high. Thin steel strips (typically 0.5 to 2.5 mm thick) traveled through the furnace at speeds of 0.5 to 2.3 m/s. These strips entered the indirect-fired section at temperatures close to 1000 K and were further heated by about 75 to 80 K. The furnace temperatures were monitored using thermocouples installed at several locations within the furnace. These temperatures were maintained within a specified operating range by intermittent firing of the radiant tubes. The reported experimental data consisted of the overall thermal efficiency of the furnace and the load surface temperatures at the inlet and exit of the furnace for varying load dimensions and velocities. The measured inlet and exit load temperatures along with the reported thermal efficiency of the furnace helped to determine the experimental net heat-transfer rate to the load.

The thermal system model for the continuous furnace was exercised for the two sets of operating conditions given in Table 3. Because in the actual furnace the radiant tubes were fired in-

Table 1 Thermophysical properties for radiant-tube continuous reheating furnace

Zone	Material	ρC, J/m^3 · K	k(a), W/m · K	ε
Load	Oxidized iron	3,518,000	$112(1 - 0.00118T + 6.9 \times 10^{-7}T^2)$	0.50
Load	AISI 347 stainless steel	3,829,400	$9.1 + 0.0175T - 1.88 \times 10^{-6}T^2$	0.85
Refractory	Firebrick	2,539,200	$1.0 + 0.0008(T - 478)$	0.75
Radiant tube	Silicon carbide			0.81

(a) Temperatures in the curve fits for k are in degrees Kelvin. Source: Ref 14, 15

Table 2 Operating conditions and dimensions for radiant-tube continuous reheating furnace

Condition or dimension	Value	Condition or dimension	Value
Ambient temperature, K	300	Furnace dimensions	
Number of radiant tubes	8 ST; 4 U; 2 W	Length (L), m	5.00
Net fuel firing rate, m^3/h	80	Height (H), m	1.35
Load velocity, m/s	0.01	Width (W), m	1.22
Load half thickness, m	0.005	Crown, side wall thickness, m	0.34, 0.23
External $\bar{h}$, W/m^2·K	10	Front, back wall thickness, m	0.23, 0.23
		Tube ID, m	0.20
		Tube OD, m	0.24

Source: Ref 14, 15

termittently, the average fuel firing rate for use in the mathematical model was computed for a given set of operating conditions from the reported overall thermal efficiency of the furnace and the experimental heat transfer to the load. The average firing rates used in the two calculations are also listed in Table 3. The U-type radiant tubes in the furnace were modeled as two straight-through tubes, with the exit conditions of the first tube set as the inlet conditions of the adjacent tube. Due to the large number of zones involved in the modeling of the entire furnace, for computational expediency the heat-transfer calculations were performed in steps by splitting the furnace into four smaller furnaces, with the exit conditions of one matching the inlet conditions of the next. The predicted temperature rise in the load for the two different operating conditions are compared with the measured inlet and exit temperatures in Fig. 4. Excellent agreement exists between predictions and measurements, with a maximum underprediction of approximately 12 °C for the exit temperature of the load. This underprediction may be due to the assumption of a steady firing condition in the mathematical model as opposed to the intermittent firing actually employed in the industrial furnace. Since radiation, which is the dominant mode of heat transfer from the radiant tubes, is a function of the fourth power of the temperature, intermittent firing of the tubes in the furnace raises the average fourth power of the tube surface temperature, resulting in higher radiative heat transfer to the load as opposed to the steady firing condition employed in the model.

Table 3 Operating conditions of the Inland Steel galvannealing furnace for validation of continuous furnace model

Condition	Set 1	Set 2
Load width, m	0.94	1.1
Load thickness, mm	1.1	1.0
Load velocity, m/s	1.05	1.14
Firing rate per tube(a), m^3/h	0.86	1.16

(a) Calculated for steady firing. Source: Ref 17

4. Continuous Furnace Parametric Investigations

The good agreement between model predictions of load surface temperature and experimental measurements in an industrial furnace provides confidence in the use of the present mathematical model as a system design and optimization tool. The model has been used to investigate the effects of design and operating parameters of the furnace on its thermal performance. Thermal performance is evaluated in terms of the overall furnace thermal efficiency and the temperature rise of the moving load in the furnace. The important parameters investigated in this study include variations in the load and refractory emis-

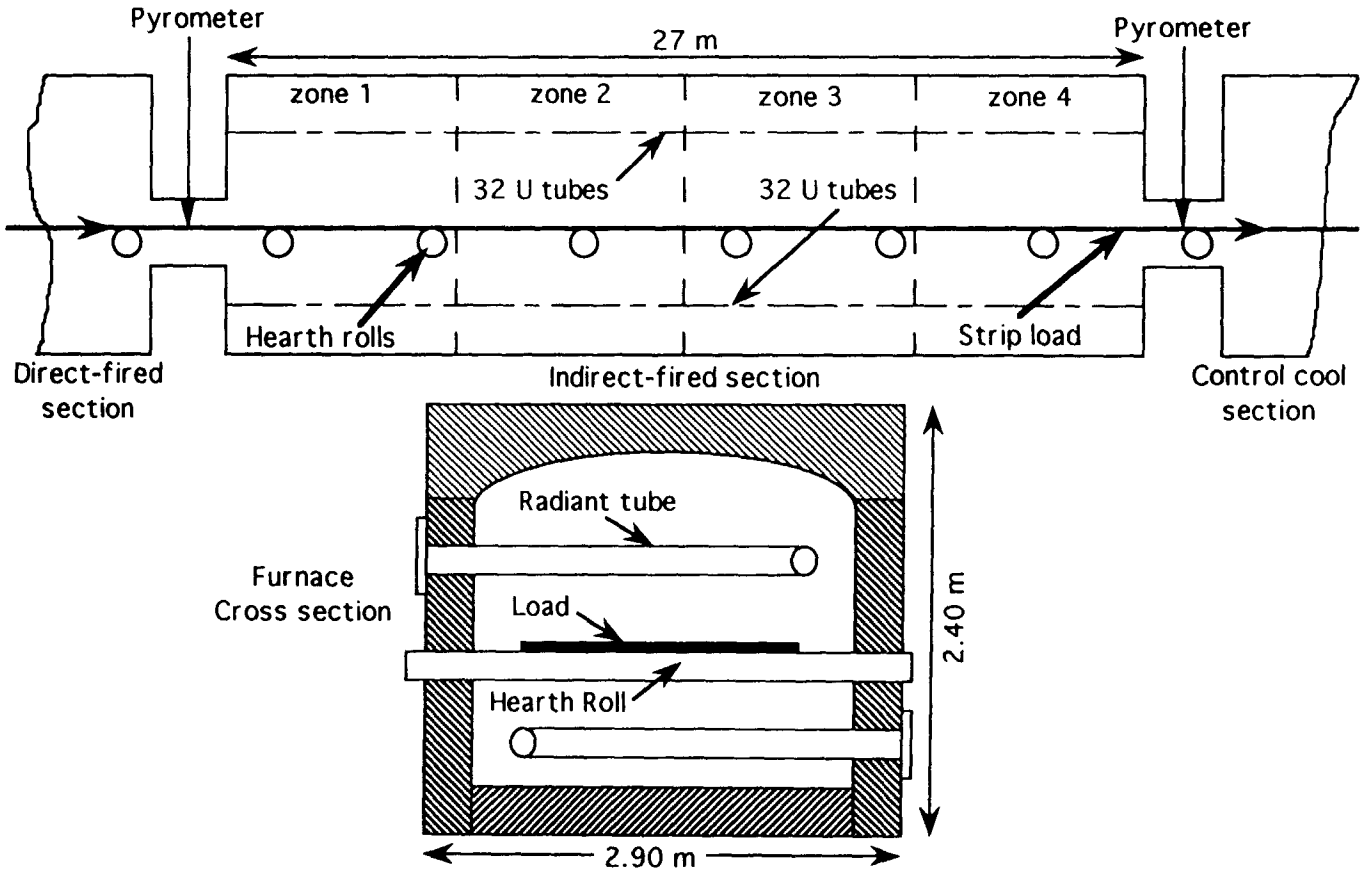

Fig. 3 Schematic of the indirect-fired section of the Inland Steel galvannealing furnace

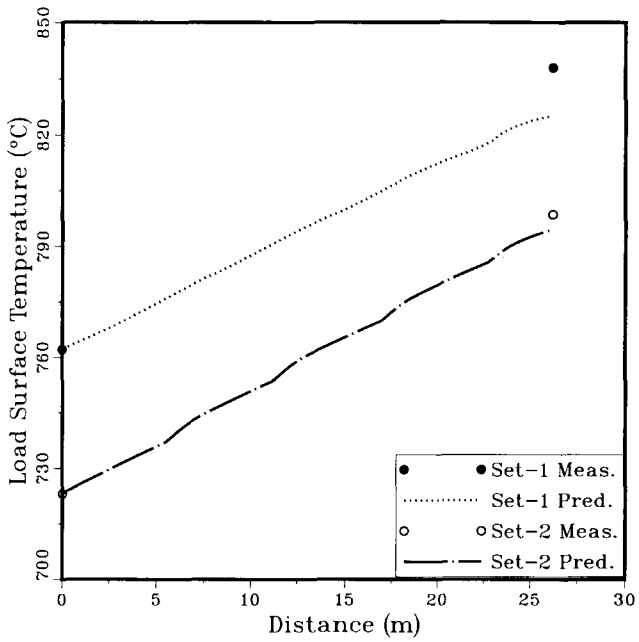

Fig. 4 Comparison of predicted load surface temperatures with measurements in the Inland Steel furnace

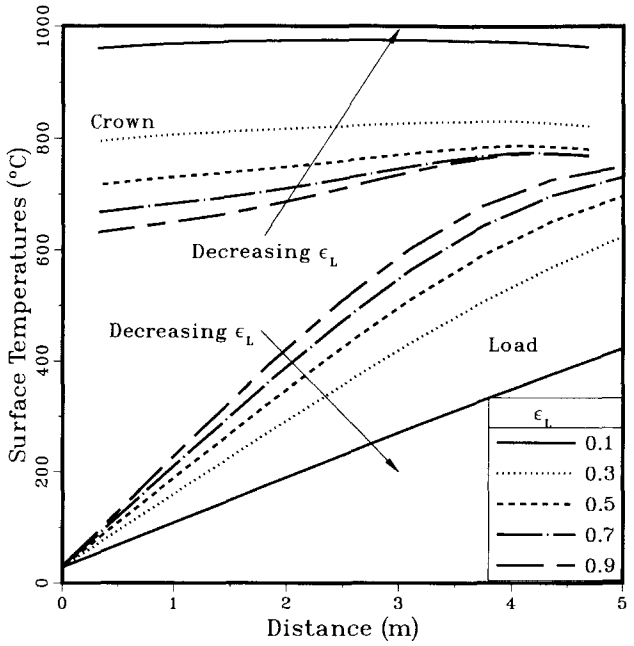

Fig. 5 Variations in the load and crown surface temperatures with distance for varying load emissivities

sivities (ε_L and ε_R) and variations in the load velocity for constant mass throughput of the load through the furnace and for constant load thickness. The parametric studies were conducted by varying each of these parameters from the baseline conditions listed in Table 2. For the numerical experiments, the load in the furnace was assumed to be oxidized iron, the thermophysical properties of which are listed in Table 1. The furnace geometry selected for the model simulations was based on the Sifco pusher-forge furnace located in Cleveland, Ohio (Ref 18). The furnace was assumed to be 5 m long and 1.22 m wide, and to consist of eight straight-through radiant tubes. The overall dimensions of the furnace and the thickness of the load and refractory walls are given in Table 2.

4.1 *Effect of Load Emissivity*

To study the effect of load emissivity on furnace thermal performance, simulations were performed by varying the load emissivity (ε_L) in the model from 0.1 (almost reflective) to 0.9 (nearly black). All other furnace parameters were maintained at the baseline values listed in Tables 1 and 2. The variations in the load surface temperature and the crown surface temperature along the length of the furnace for different values of load emissivity are plotted in Fig. 5. The load surface temperature increases with increasing load emissivities, whereas the crown surface temperature decreases. The increase in load surface temperature can be attributed to the increased absorption of radiant energy at the load surface with increasing load emissivities. Because the additional radiant energy at the load surface is absorbed from the crown surface, it results in a corresponding decrease in the crown temperature. For low values of ε_L the increase in load surface temperature is almost linear, whereas at higher values the load appears to asymptotically approach a maximum temperature at the exit of the furnace. The maximum temperature attainable by the moving load is governed primarily by the firing conditions in the radiant tubes and the thermophysical properties of the load. Although substantial increases in load surface temperatures are obtained by raising the load emissivity at nearly reflective conditions, the increase becomes less pronounced as the load surface approaches a nearly black condition. This implies that the furnace thermal efficiency, which is defined as

$$\eta_{overall} = \frac{\text{Net heat input to load}}{\text{Net heat released due to combustion}} \qquad \text{(Eq 30)}$$

increases substantially with load emissivity for nearly reflective surfaces and increases only slightly for near-black surfaces.

Figure 5 also shows that the crown surface temperature is a minimum at the point where the load enters the furnace and progressively increases toward the exit. This arises due to large amounts of energy being transferred from the crown to the cold load at the furnace entrance. From the point of view of furnace operation, the decreased crown surface temperature is advantageous, reducing furnace heat losses and improving furnace service life.

4.2 *Effect of Refractory Emissivity*

The effect of refractory emissivities on furnace thermal performance was simulated by varying ε_R from 0.1 to 0.9 and maintaining the rest of the furnace parameters at the values listed in Tables 1 and 2. The variations in the load and the crown surface temperatures for varying values of ε_R are shown in Fig. 6. Although the variations in ε_R seem to have negligible effect on the load surface temperature, the crown surface temperature

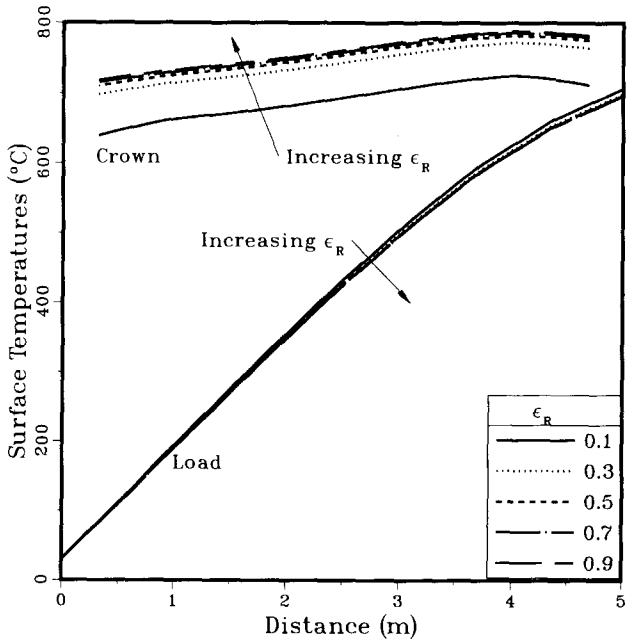

Fig. 6 Variations in the load and crown surface temperatures with distance for varying refractory emissivities

increases with increasing refractory emissivities. As the refractory emissivity increases, radiant energy absorbed by the crown increases, resulting in the rise in crown surface temperature. From Fig. 6, it is again evident that substantial increases in the crown surface temperature are obtained by increasing ε_R for nearly reflective refractories.

The refractory surfaces transfer radiant energy to the load via two processes: (1) reflection of the incoming radiant energy from the other surfaces of the enclosure and (2) absorption of the incoming energy and reradiation to the load. Thus, highly reflective refractories transfer energy to the load by reflection of incident radiation, while black refractories absorb incident energy and reradiate to the load. Thus, as shown in Fig. 6, variations in refractory emissivity do not significantly alter the load temperatures. Since the net heat transfer to the load is nearly independent of ε_R, the overall thermal efficiency of the furnace (Eq 30) is not expected to vary with changes in refractory emissivities.

The variations of enclosure and overall furnace efficiencies with load and refractory emissivities are plotted in Fig. 7. The other furnace parameters are held fixed at the values presented in Tables 1 and 2. The enclosure efficiency is defined as the ratio of the net heat flux incident on the load to the net heat flux leaving the radiant-tube walls. Thus, while the enclosure efficiency quantitatively describes the percent fractional heat losses from the furnace enclosure alone, the overall thermal efficiency additionally includes the heat losses via the radiant-tube exhaust. As discussed earlier, Fig. 7 indicates that the furnace efficiencies are unaffected by changes in refractory emissivities. However, furnace efficiencies increase progressively with increases in load emissivity, with substantial increases occurring at nearly reflective load conditions. The large difference between the enclosure and overall efficiencies is noteworthy.

4.3 *Effect of Load Velocity*

The rate of throughput of stock material in a furnace is very important in terms of productivity. Although a decrease in load velocity (increased residence time in the furnace) may improve heating of the load, it may also increase production time and costs. Therefore, the effects of varying the load velocity were studied for a constant as well as a varying mass throughput of the load in the furnace. For the first set of simulations, the thermal performance of the furnace was evaluated by maintaining the load throughput at a constant value of 0.96 kg/s, while the load velocities were varied from 0.001 to 0.5 m/s. The constant mass throughput for varying load velocities was achieved by adjusting the thickness of the stock material accordingly. Thus, at higher load velocities the thickness of the stock material was correspondingly reduced.

The effect of varying load velocities on the load and crown surface temperatures for constant load throughput in the furnace is plotted in Fig. 8. Varying the load velocities at constant mass throughput has little effect on the load and crown surface temperatures and hence on the thermal performance of the furnace. The net heat-transfer rate to the load can be expressed in terms of the load temperature rise as:

$$Q_L = \dot{m}_L C_L \Delta T_m \qquad \text{(Eq 31)}$$

where ΔTm is the mean temperature rise of the load from the inlet to the exit of the furnace. In the present simulations, the mass throughput $\dot{m}_L$ is maintained constant, and Q_L is a function of the unaltered surface properties of the furnace enclosure; therefore, the temperature rise for varying load velocities in Eq 31 remains a constant. Thus, if the throughput is maintained constant, the residence time in the furnace can be significantly reduced by increasing the load velocities with no adverse effects on the thermal performance of the furnace.

4.4 *Effect of Load Velocity for Constant Load Thickness*

The effect of varying load velocities for constant load thickness is studied by varying load velocities from 0.008 to 0.1 m/s. The variations in the load surface temperature and the net heat flux to the load for these conditions are plotted in Fig. 9 and 10, respectively. As expected, the load surface temperature increases with decreasing load velocity due to longer residence time of the load within the furnace. This is also apparent from Eq 31. The net heat-transfer rate to the load remains more or less a constant, whereas decreasing load velocity decreases $\dot{m}_L$, resulting in a corresponding increase in load temperatures. The decreasing load velocity, however, reduces the production rate in practical applications. Hence, for a specific heating situation, the load velocity needs to be optimized in order to achieve a satisfactory balance between production rate and higher load exit temperatures or better furnace thermal performance.

The net heat flux to the load, plotted for various load velocities in Fig. 10, shows a highly nonuniform heating of the load at lower load velocities. At the furnace inlet, the load surface is

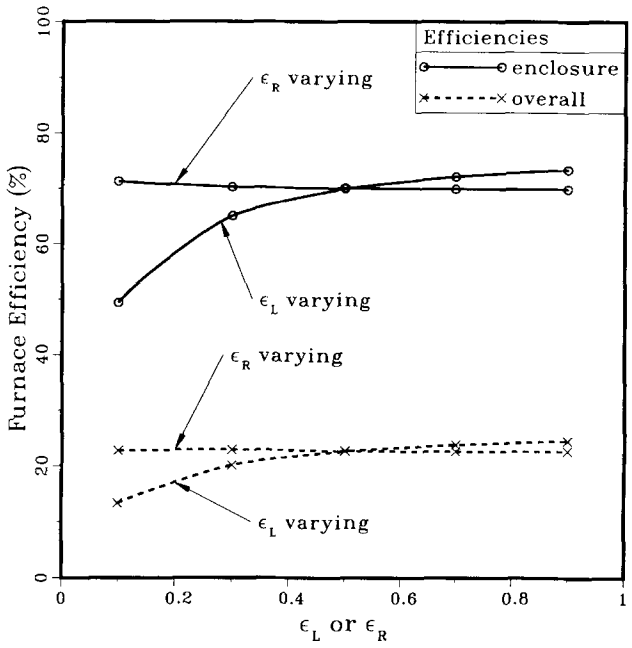

Fig. 7 Variations in the furnace thermal efficiencies with load and refractory emissivities

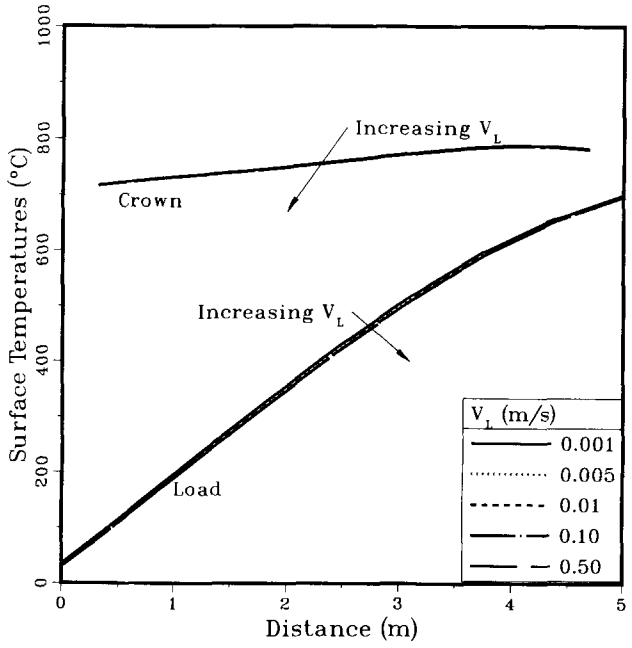

Fig. 8 Variations in the load and crown surface temperatures with distance for varying load velocities ($\dot{m}_L$ = constant)

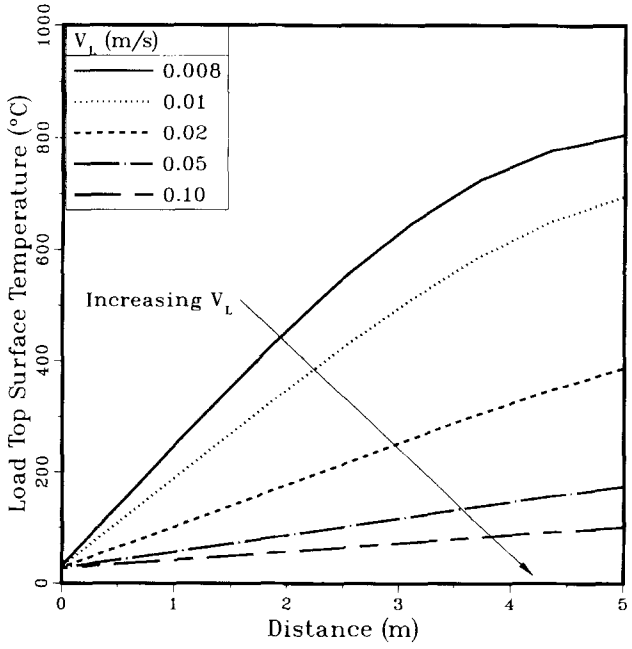

Fig. 9 Variations in the load and crown surface temperatures with distance for varying load velocities (t_L = constant)

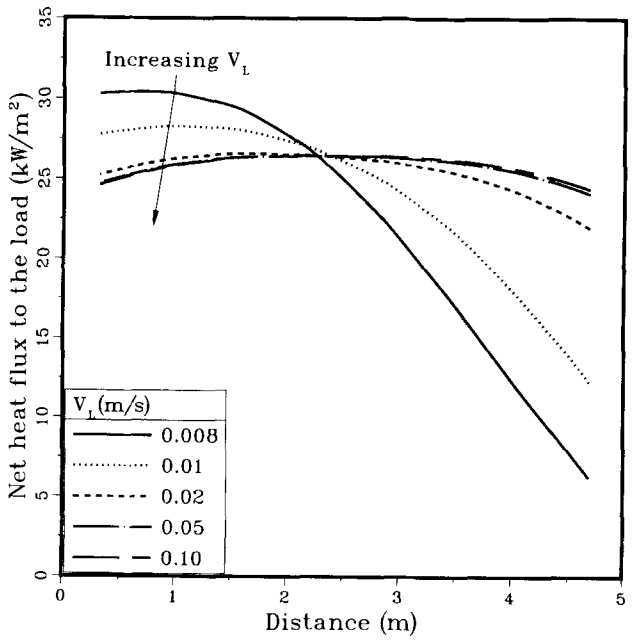

Fig. 10 Variations in the net heat flux to the load with distance for varying load velocities (t_L = constant)

relatively cold, and thus a large amount of heat is transferred to the load by radiation. However, at lower load velocities, the longer residence time (L_L/V_L) causes the load surface temperature to approach the temperature of the radiant tubes. At the furnace exit, therefore, the net heat flux from the radiant tubes to the load decreases significantly, as represented by the solid line for a load velocity of 0.008 m/s in Fig. 10. For higher load velocities, the load surface temperature increase between inlet and outlet is much smaller (by about 100 °C for a V_L of 0.1 m/s). Because these temperatures are much lower than the radiant-tube temperatures, the net heat flux to the load remains more or less uniform (Fig. 10). The net heat-transfer rate to the load can be estimated from the area enclosed beneath the heat flux curves in Fig. 10. A qualitative comparison of these areas indicates that the net heat-transfer rate to the load for the simulations is more or less a constant.

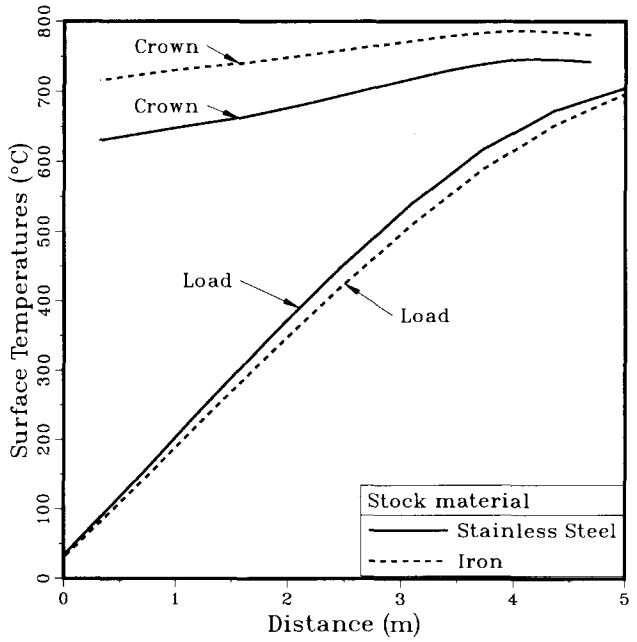

Fig. 11 Variations in the load and crown surface temperatures with distance for two different stock materials in the furnace

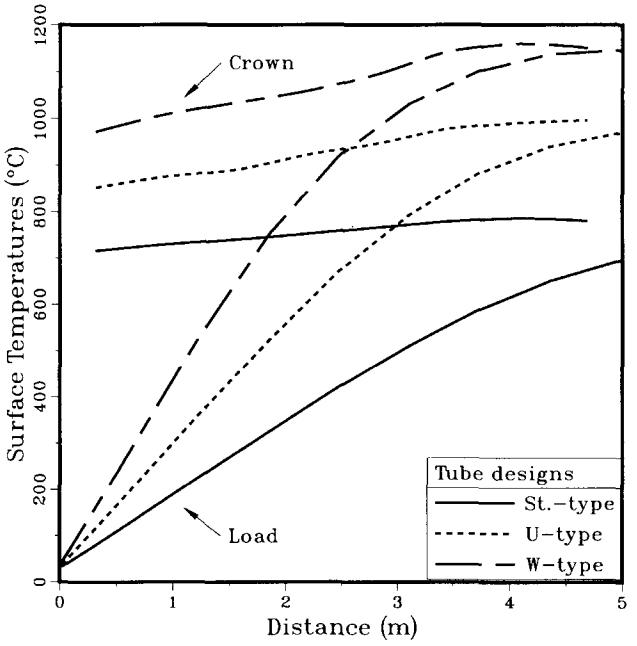

Fig. 12 Variations in the load and crown surface temperatures with distance for different radiant-tube designs in the furnace

4.5 *Effect of Stock Material*

The capabilities and flexibility of the mathematical model are demonstrated by comparing the results of the furnace model simulations for two different stock materials in the furnace. The two stock materials heated in the furnace were AISI 347 stainless steel and oxidized iron, the thermophysical properties of which are listed in Table 1 (Ref 14, 15). Temperature-dependent thermal conductivity was used for both materials, and the thickness and velocity of the steel and iron strips were assumed to be the same in the simulations. The mass throughput of the stainless steel strip was thus about 1.3% higher than that of iron. The emissivity of the steel strip in the simulations was assumed to be 0.85 (Ref 14), and that of the iron strip was 0.50 (Ref 15). The load surface temperature and the furnace crown surface temperature variations during the heating of the two different stock materials in the furnace are plotted in Fig. 11. Despite the higher mass throughput and higher specific heat, the steel sheet heats up faster than the iron sheet. This is due to the higher emissivity of steel compared to that of iron, which causes higher heat transfer to the load in the furnace. The higher emissivity of steel correspondingly decreases the crown surface temperatures by about 10% compared to the heating of iron in the furnace. Calculations such as these can provide the furnace designer or operator information about the important furnace parameters and operating conditions necessary to achieve optimum thermal performance and productivity with different stock materials.

4.6 *Effect of Tube Designs*

To study the effect of radiant-tube designs on furnace performance, three different radiant-tube designs were considered in the simulations: the straight-through type, the U-type, and

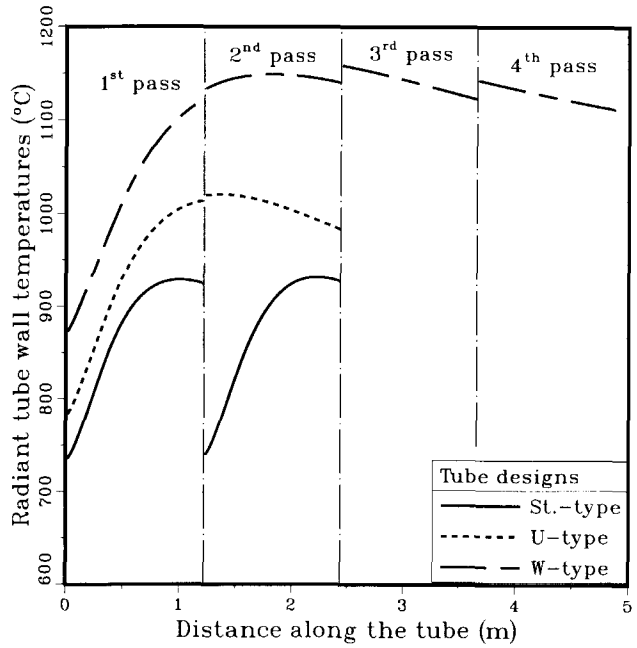

Fig. 13 Axial variations in the radiant-tube wall temperatures for different radiant-tube designs in the furnace

the W-type. In U-type and W-type radiant tubes, fuel and air enter one leg of the tube via a diffusion flame burner; the products of combustion pass through the U- and W-shaped sections, respectively, eventually exiting via the exhaust branch of the tube. In the thermal system model, the different branches of the U-type and W-type tubes were simulated as individual straight-through tubes by setting the exit conditions of one tube as the inlet conditions of the next. Thus, the U-type radiant tube was

simulated as two straight-through tubes and the W-type radiant tube as four straight-through tubes. The rate of fuel burnup in the tubes was obtained using the fuel burnup correlation proposed by Lisienko et al. (Ref 10) (Eq 19). The net fuel firing rate into the furnace for each simulation was maintained at 80 m^3/h by distributing the fuel evenly to the different tubes. Thus, in each of the eight straight-through radiant tubes, the firing rate was 10 m^3/h; in each of the four U-type tubes, 20 m^3/h; and in each of the two W-type tubes, 40 m^3/h.

Figure 12, which shows the variations in the load surface temperature for the same net fuel firing rate in the radiant tubes, indicates that the load surface temperatures are the highest for the W-type tube design, followed by the U-type and then the straight-through tubes. The lower load surface temperatures for the straight-through tubes in the furnace is due to the incomplete burning of fuel in the radiant tubes. A considerable amount of energy is lost in the form of unburned fuel at the exhaust of the straight-through tube. However, in the U-type and W-type tubes, further burning of the unburned fuel from the first branch takes place, resulting in a higher average tube wall temperature in the successive branches of the tube.

The variations in the radiant-tube wall temperatures along the axial length of the tube for the straight-through, U-type, and W-type tubes are plotted in Fig. 13. For the purposes of com-

NOMENCLATURE

AF	air-to-fuel ratio	N	number of radiant tubes
AR	area ratio	Nu	Nusselt number, hD/k
C	specific heat of solid, J/kg·K	p	pressure, N/m^2
C_p	specific heat of fluid, J/kg·K	P	perimeter, m
D	diameter, m	P_r	momentum ratio
f_D	Darcy friction factor	Pr	Prandtl number, $\mu C_p/k$
F_{k-j}	configuration factor between kth and jth surfaces	q	heat flux, W/m^2
		Q	heat-transfer rate (Fig. 2), W
h	convective heat-transfer coefficient, $W/m^2 \cdot K$	r	radial coordinate, m
$\bar{h}$	external effective heat transfer coefficient accounting for radiative and convective heat transfer, $W/m^2 \cdot K$	R	radius, m
		Ra	Rayleigh number
		Re	flow Reynolds number, $\rho VD/\mu$
h^a	sensible enthalpy, J/kg	s	number of surfaces in contact with a gas volume zone
H	height, m		
ΔH_{fu}	heat of combustion of fuel, J/kg	S	distance between radiant tubes (Fig. 1), m
J	radiosity at a surface, W/m^2	t	thickness, m
k	thermal conductivity, W/m·K	T	absolute temperature, K
L	length, m	V	velocity, m/s
$\dot{m}$	mass flow rate, kg/s	W	width, m
M	total number of surface zones	x, y, z	coordinates
n	normal direction	Δz	axial step size, m

Greek characters

α	absorptance	μ	viscosity, $N \cdot s/m^2$
δ_{kj}	Kronecker delta: $\delta = 1$ when $k = j$; $\delta = 0$ when $k \neq j$	Φ	equivalence ratio, AF_{st}/AF
		ρ	density, kg/m^3
ε	surface emissivity; gas emittance	σ	Stefan-Boltzmann constant, $W/m^4 \cdot K$
η	efficiency	τ	shear stress, N/m^2
κ	fuel burnup coefficient		

Subscripts

a	air	o	outer
c_L	centerline	ox	oxidant
cg	combustion gas	pr	products
conv	convection	r	radial
D	diameter	rad	radiation
en	enclosure	ref	reference
fu	fuel	st	stoichiometric
FT	based on stoichiometric adiabatic flame temperature	t	tube
		tw	tube wall
g	furnace gas	tot	total
i	inner	w	wall
L	load	z	axial

parison, the radiant-tube temperatures in two adjacent straight-through tubes are plotted together. Figure 13 clearly indicates that the average tube wall temperature of the exhaust branch of the U-type tube is higher than that of the second straight-through tube. The higher average tube wall temperature in the exhaust branch of the U-type tube is the result of the high-temperature exhaust gases and unburned fuel of the first branch entering this section and causing further burning of the fuel. Overall, the tube wall temperatures of the W-type radiant tube are the highest, which explains the higher heat transfer to the load for the W-type design. The study of furnace thermal performance for different radiant-tube designs indicates the superiority of the W-type tube over U-type and straight-through radiant tubes for the same net fuel input into the furnace.

5. Conclusions

The mathematical model of the radiant-tube continuous furnace developed in this study can be conveniently used as a design and diagnostic tool for industrial heat-treating operations. The detailed parametric analysis of the continuous furnace revealed important trends and design conditions for the furnace. The analysis indicated that load emissivity is a very important model parameter that affects the thermal performance of the furnace (see Fig. 5 and 7).

Based on the particular furnace design and operating conditions considered in this study, the conclusions can be summarized as follows:

- Increasing load emissivity enhances heat transfer to the load and substantially reduces crown temperatures, thereby reducing furnace heat losses. The furnace efficiency also increases with increasing load emissivity. This suggests that coating a low-emissivity stock with a high-emissivity coating that does not significantly affect the properties of the stock material can make the furnace heating operation more efficient.
- Although the refractory emissivity has no adverse effect on overall furnace efficiency, highly reflecting refractories reduce the temperature of the refractories and hence improve their operating life.
- Varying the load velocity at constant mass throughput of the load does not significantly affect furnace operation. However, higher load velocities lead to more uniform load exit temperatures due to a decrease in the thickness of the load.
- The load velocity at constant load thickness needs to be optimized for best production rate and optimum heating rate in the furnace.
- A comparison of the thermal performance of the furnace for two different stock materials revealed that if the thermal performance of the furnace is optimized for specific stock material, the performance may be significantly altered when the stock material in the furnace is changed.
- Analysis of the thermal performance of the continuous furnace for three different radiant-tube designs showed the W-type design to be superior to the U-type and straight-through designs for the same net fuel firing rate in the tubes.

Acknowledgments

Financial assistance for this project was provided by the Gas Research Institute, Chicago, Illinois (Contract No. 5086-260-1293), and is gratefully acknowledged. The authors would like to thank Dr. F. Fish of the Gas Research Institute for his interest and support, and Mr. D.A. White of Inland Steel Corporation for providing operating data on the radiant-tube continuous furnace.

References

1. R. Pritchard, J.J. Guy, and N.E. Connor, *Handbook of Industrial Gas Utilization*, Van Nostrand Reinhold, 1977
2. R.F. Harder, S. Ramadhyani, and R. Viskanta, "Gas-Fired Radiant Tubes: A Review of Literature," Topical Report No. GRI-87/0343, Gas Research Institute, 1987
3. R.F. Harder, S. Ramadhyani, and R. Viskanta, Evaluation and Modeling of Gas-Fired Radiant Tubes, *Modeling of Combustion Systems: 1988 National Heat Transfer Conference*, Vol 96, American Society of Mechanical Engineers, 1988, p 67-77
4. H.C. Hottel and A.F. Sarofim, *Radiative Transfer*, McGraw-Hill, 1967
5. R. Siegel and J.R. Howell, *Thermal Radiation Heat Transfer*, 3rd ed., McGraw-Hill, 1992
6. H. Ramamurthy, S. Ramadhyani, and R. Viskanta, Thermal System Model for a Radiant Tube Batch Reheating Furnace, *Proceedings of the 1992 International Gas Research Conference*, Vol 2, H.A. Thompson, Ed., Government Institutes Inc., 1992, p 2205-2216
7. H. Ramamurthy, S. Ramadhyani, and R. Viskanta, Modeling of Heat Transfer in Indirectly-Fired Continuous Reheating Furnace, *Transport Phenomena in Materials Processing*, HTD-Vol 146, P.J. Bishop et al., Ed., American Society of Mechanical Engineers, 1990, p 37-46
8. H. Ramamurthy, "Analysis of Energy Transfer in Industrial Gas-Fired Radiant Tube Furnaces," Ph.D. thesis, Purdue University, 1993
9. H. Ramamurthy, S. Ramadhyani, and R. Viskanta, A Two-Dimensional Axisymmetric Model for Combusting, Reacting and Radiating Flows in Radiant Tubes, *J. Inst. Energy*, in press
10. V.G. Lisienko, F.R. Skylar, Y.V. Dryuchenkov, L.N. Toritsyn, V.V. Vokov, and A. Tikhotskii, Combined Solution of the Problem of External Heat Transfer and Heat Transfer Inside a Gas Radiation Tube for Thermal Furnaces with a Protective Atmosphere, *J. Eng. Phys.*, Vol 50 (No. 1), 1986, p 70-76
11. V. Gnielinski, New Equations for Heat and Mass Transfer in Turbulent Pipe and Channel Flows, *Int. Chem. Eng.*, Vol 16 (No. 2), 1976, p 359-367
12. H.C. Hottel, "Radiation from Carbon Dioxide, Water Vapor and Soot," presented to the American Flame Research Committee, 1985
13. V.T. Morgan, The Overall Convective Heat Transfer from Smooth Circular Cylinders, *Advances in Heat Transfer*, Vol 11, T.F. Irvine, Jr. and J.P. Hartnett, Ed., Academic Press, 1975, p 199-264
14. F.P. Incropera and D.P. DeWitt, *Fundamentals of Heat and Mass Transfer*, John Wiley & Sons, 1985
15. E.M. Sparrow and R.D. Cess, *Radiation Heat Transfer*, Brooks/Cole Publishing, 1970
16. S.V. Patankar, *Numerical Heat Transfer and Fluid Flow*, Hemisphere, 1980
17. D.A. White, Inland Steel Corporation, personal communication, 1993
18. D.W. Bodkins, Columbia Gas System Service Corporation, personal communication, 1993